

Numerical study of plasmon properties in the SU(2)-Higgs model

Wai Hung Tang* and Jan Smit†

Institute of Theoretical Physics, University of Amsterdam
Valckenierstraat 65, 1018 XE Amsterdam, the Netherlands

December 2, 2024

Abstract

Using the (effective) classical approximation, we compute numerically time-dependent correlation functions in the SU(2)-Higgs model around the electroweak phase transition, for $m_H \approx m_W$. The parameters of the classical model have been determined previously by the dimensional reduction relations for time-independent correlators. The H and W correlation functions correspond to gauge invariant fields. They show damped oscillatory behavior from which we extract plasmon frequencies ω and damping rates γ . In the Higgs phase γ_H and γ_W have roughly the value obtained in analytic calculations. In the confinement phase (where analytic estimates for gauge invariant fields are not available), γ_H (γ_W) is an order of magnitude larger (smaller) than in the Higgs phase. The frequency ω_H shows a clear dip at the transition, while ω_W appears to become very small in the confinement phase. We find good evidence that the results are approximately lattice spacing independent, which we take as sign of good health of the classical approximation.

*email: tang@phys.uva.nl

†email: jsmit@phys.uva.nl

1 Introduction

The classical approximation has been introduced some time ago in quantum field theory to avoid the difficulties of numerical simulations of time dependent phenomena at high temperature [1]. It is potentially a very powerful method for nonequilibrium phenomena as well. It has been used for the numerical study of the Chern-Simons diffusion rate in the (1+1)D abelian Higgs model [2–7], the (3+1)D SU(2)-Higgs model [8, 9, 10] and pure SU(2) gauge theory [11], as well as in a study of real time properties of the electroweak phase transition [12]. The results have been encouraging. For example, the sphaleron rate in the classical abelian Higgs model obtained by numerical simulations agrees with the analytic expression of quantum field theory [4–7], and in the corresponding pure SU(2) and SU(2)-Higgs cases the rate appears to be lattice spacing independent [11, 10]. On the other hand, the classical results for the rate are puzzling in the high temperature region of the abelian model [7] and the analytical sphaleron rate in the Higgs phase of the SU(2)-Higgs model is in disagreement with results of recent numerical simulations [9, 10]. This may be due to bad ultraviolet properties of the observable used for estimating the Chern-Simons diffusion [9], suggesting a tricky situation where approximate lattice spacing independence is no guarantee for physical results. In the corresponding case of the topological susceptibility in euclidean lattice QCD such an unfavorable situation is indeed possible, see e.g. Fig. 7 in ref. [13]. Apart from this, also the very validity of the effectively¹ classical approximation for real time processes needs further clarification.

For this reason we undertook the present study of correlation functions in the classical SU(2)-Higgs theory. The emphasis here is on time dependent correlation functions. The static correlation functions, which describe the initial conditions of the time dependent ones, have been well studied since they correspond to a dimensional reduction approximation of the quantum theory at high temperature. The static theory can be renormalized, with finite renormalizations determined by matching the classical to the quantum theory [14]. An important question is if the time dependent theory is also renormalizable.

Recently [15], time dependent correlation functions have been studied in hot classical ϕ^4 theory using perturbation theory and it was shown that the ultraviolet divergencies can be absorbed in counterterms, the same mass counterterms as needed in the static theory. This led in particular to a finite classical plasmon damping rate. Matching the parameters of the classical static theory with those in the quantum theory, this classical damping rate was found to agree with the hard thermal loop expression of the quantum theory. Such matching was applied previously to the SU(2)-Higgs model for the computation of the Chern-Simons diffusion rate [10]. The analysis is still to be completed by a more detailed

¹By ‘classical’ we shall always mean ‘effectively classical’ in this paper, i.e. in terms of a classical action with effective coupling constants.

comparison between the fully time dependent classical and quantum theories.

Our approach is different from propositions based on an effective theory of hard thermal loops [27, 28, 29], in which the cutoff of the classical theory should not be removed. We are instead assuming that the classical SU(2)-Higgs theory is renormalizable (as in the scalar case [15]) and that physical results are free of regularization artefacts, for sufficiently large cutoff or small lattice spacing. To test this assumption numerically we concentrate on relatively simple time dependent correlation functions. First of all, we want to see if it is feasible to compute such autocorrelation functions numerically with reasonable accuracy, find out if the results are compatible with lattice spacing independence, using the counterterms known from the static theory, and compare with hard thermal loop results.

Such a comparison is not straightforward in the high temperature phase. In the analytic calculations the correlation functions are constructed from the elementary field variables using gauge fixing, while nonperturbatively one tends to use gauge invariant composite local fields. Even if the final results obtained analytically are gauge invariant, it is not clear that these refer to the same quantities as those obtained with the gauge invariant fields. For example, in the confinement phase there is a large discrepancy between the two cases in the screening masses with W quantum numbers [16–21] (see also the reviews [22, 23]). In the Higgs phase the results agree, as can be understood from the usual argument which we now review.

The simplest gauge invariant composite fields (which we also use) read in the continuum

$$H = \varphi^\dagger \varphi, \quad \varphi = \begin{pmatrix} \varphi_u \\ \varphi_d \end{pmatrix}, \quad (1)$$

$$W_\mu^\alpha = i \text{Tr} \phi^\dagger (\partial_\mu - i A_\mu^\beta t_\beta) \phi t_\alpha, \quad \phi = \begin{pmatrix} \varphi_d^* & \varphi_u \\ -\varphi_u^* & \varphi_d \end{pmatrix}, \quad (2)$$

with φ the Higgs doublet, A_μ^α the gauge fields and $t_\alpha = \tau_\alpha/2$ the SU(2) generators. In the Higgs phase these fields correspond to the usual Higgs and gauge fields. Since $\phi = \sqrt{H} V$ with $V \in SU(2)$, W_μ^α is essentially the gauge field in the unitary gauge $V = 1$, as can be seen in perturbation theory by replacing φ by its vacuum expectation value, neglecting fluctuations. This is not useful in the confinement phase where the theory behaves like QCD and perturbation theory runs into infrared problems. Nonperturbatively H and W_m^α ($m = 1, 2, 3$) are primarily characterized by their behavior under spatial rotations and weak isospin: (scalar, scalar) and (vector, vector), respectively. We have not studied the time component W_0^α , which transforms as (scalar, vector).

To get an idea of the properties of the system being simulated we also computed static correlators of H and W and estimated their screening masses. The

temperatures varied around the electroweak transition and parameters were furthermore chosen such that for the zero temperature masses $m_H \approx m_W$. From the time dependent correlation functions we then attempted to extract plasmon frequencies and damping rates of H and W .

2 Classical SU(2)-Higgs model at finite temperature

We use the same notation as in [10]. The classical SU(2)-Higgs model is defined on a spatial lattice with lattice distance a . The parallel transporters (lattice gauge field) are denoted by $U_{m\mathbf{x}}$, $D_m \bar{\varphi}_{\mathbf{x}} = U_{m\mathbf{x}} \bar{\varphi}_{\mathbf{x}+\hat{m}} - \bar{\varphi}_{\mathbf{x}}$ is the covariant lattice derivative acting on the lattice Higgs doublet $\bar{\varphi}_{\mathbf{x}}$, $U_{mn\mathbf{x}}$ is the product of parallel transporters around the plaquette $(\mathbf{x}mn)$. The canonical momenta in the temporal gauge are denoted by $\bar{\pi}$, $\bar{\pi}^\dagger$ and \bar{E}_m^α , with nontrivial Poisson brackets

$$\{U_{m\mathbf{x}}, \bar{E}_{m\mathbf{x}}^\alpha\} = iU_{m\mathbf{x}}\tau_\alpha, \quad \{\bar{\varphi}_{\mathbf{x}}, \bar{\pi}_{\mathbf{x}}^\dagger\} = 1. \quad (3)$$

The effective classical hamiltonian is given by

$$\frac{H_{\text{eff}}}{T} = \bar{\beta} \bar{H}, \quad (4)$$

$$\begin{aligned} \bar{H} = \sum_{\mathbf{x}} [& \frac{1}{2} z_E \bar{E}_{m\mathbf{x}}^\alpha \bar{E}_{m\mathbf{x}}^\alpha + z_\pi \bar{\pi}_{\mathbf{x}}^\dagger \bar{\pi}_{\mathbf{x}} + \sum_{m < n} (1 - \frac{1}{2} \text{Tr } U_{mn\mathbf{x}}) \\ & + (D_m \bar{\varphi}_{\mathbf{x}})^\dagger D_m \bar{\varphi}_{\mathbf{x}} + \bar{\lambda} (\bar{\varphi}_{\mathbf{x}}^\dagger \bar{\varphi}_{\mathbf{x}} - \bar{v}^2)^2], \end{aligned} \quad (5)$$

where T is the temperature and $\bar{\beta}$, $\bar{\lambda}$ and \bar{v}^2 are effective couplings which depend on a , T and the couplings in the 4D quantum theory,

$$\bar{\beta} \approx \frac{4}{g^2 a T}, \quad \bar{\lambda} \approx \frac{m_H^2}{2m_W^2}, \quad (6)$$

$$\begin{aligned} 4\bar{\lambda}\bar{v}^2 = a^2 T^2 \left[\frac{m_H^2}{T^2} - \left(\frac{3}{2} g \right)^2 \left(\frac{3+\rho}{18} - \frac{3+\rho}{3} \frac{2\Sigma}{aT} \right) \right. \\ \left. - \left(\frac{3}{2} g \right)^4 \frac{1}{8\pi^2} \left(\frac{149+9\rho}{486} + \frac{27+6\rho-\rho^2}{27} \ln \frac{aT}{2} - \frac{27\eta+6\rho\bar{\eta}-\rho^2\tilde{\eta}}{27} \right) \right], \end{aligned} \quad (7)$$

$$\Sigma = 0.252731. \quad (8)$$

Here $\rho = m_H^2/m_W^2$ and g and m_H are parameters in the MS-bar scheme at scale $\mu_T \equiv 4\pi \exp(-\gamma_E)T \approx 7T$. These relations follow from matching the static classical theory to the dimensionally reduced quantum theory [10], using the results of ref. [25]. As in [10] we set $z_E = z_\pi = 1$. The implementation of these parameters has to wait for a detailed matching between the time dependent classical and quantum theories.

$\bar{\beta}_c$	N	β_H^c	\bar{v}_c^2	T_c/m_H
12	20	0.347733	0.26295	2.14
12	24	0.34772	0.26273	2.15
20	32	0.34173	0.15597	2.15

Table 1: Critical values of $(\bar{\beta}, \bar{v})$ for $\bar{\lambda} = 1/2$. The values of T_c/m_H were calculated using eq. (7).

The equations of motion follow from the above hamiltonian and Poisson brackets. The initial conditions are distributed according to the classical partition function

$$Z = \int DEDUD\pi D\varphi \left[\prod_{\mathbf{x}\alpha} \delta(G_{\mathbf{x}}^\alpha) \right] \exp(-H_{\text{eff}}/T), \quad (9)$$

where $\delta(G_{\mathbf{x}}^\alpha)$ enforces the Gauss constraint, which is part of the temporal gauge formalism. Time dependent correlation functions of observables O are defined by averaging $O(t)O(0)$ over initial configurations,

$$\langle O(t)O(0) \rangle = \frac{1}{Z} \int DEDUD\pi D\varphi \left[\prod_{\mathbf{x}\alpha} \delta(G_{\mathbf{x}}^\alpha) \right] \exp(-H_{\text{eff}}/T) O(t)O(0). \quad (10)$$

Examples of such observables are the simple gauge invariant fields we use to study the W and Higgs excitations:

$$W_{m\mathbf{x}}^\alpha = i\text{Tr} \phi_{\mathbf{x}}^\dagger U_{m\mathbf{x}} \phi_{\mathbf{x}+\hat{m}} \tau_\alpha, \quad (11)$$

$$H_{\mathbf{x}} = \bar{\varphi}_{\mathbf{x}}^\dagger \bar{\varphi}_{\mathbf{x}}. \quad (12)$$

The static system (i.e. the system described by the classical partition function at time zero) is believed to be well understood because of its connection with dimensional reduction. For given \bar{v}^2 and relatively small $\bar{\lambda}$ there is a critical value of $\bar{\beta}$, above which the system is in the Higgs phase and below which it is in the confinement phase. The transition is of first order [25], weakening in strength as m_H/m_W increases, and turning into a crossover near $m_H \approx m_W$ [26].

As in [10], we have chosen $\bar{\lambda} = 1/2$, which means $m_H/m_W \approx 1$. The transition is then still clearly visible, especially in the rate of Chern-Simons diffusion [10]. Accordingly set $\rho = 1$ in the application of eq. (7). We also neglect the running of g and m_H with temperature, and choose $g = 2/3$, which implies $aT = 9/\bar{\beta}$. For given \bar{v}^2 eq. (7) then gives T/m_H as a function of $\bar{\beta}$.

Keeping instead T/m_H fixed while increasing $\bar{\beta}$ and changing \bar{v}^2 according to (7) should get us closer to the continuum limit. Physical quantities of the static theory then become $\bar{\beta}$ independent. It is not clear at this point if the same holds for physical quantities related to the full time dependent theory, such as plasmon masses and rates.

Table 1 shows some pseudo critical values $\bar{\beta}_c$ and \bar{v}_c^2 on lattices of size N^3 . These values are obtained by a translation of the dimensional reduction results of [25] into the parameterization used here in terms of $\bar{\lambda}$ and \bar{v}^2 . For the record we mention the connection with the parameterization used in [25]: $\bar{\beta} = \beta_G$, $\bar{\lambda} = 4\beta_G\beta_R/\beta_H^2$, $(\bar{v}^2/\bar{\lambda}) = 4(3\beta_H - 2\beta_R - 1)/\beta_H$, $\beta_2^A = \beta_4^A = 0$. The last two parameters were not zero in the action used in [25], but the difference does not seem to be important for the location of the phase transition [10].

3 Numerical computation

We use the algorithm and numerical implementation offered in ref. [24]. A simulation consisted of alternating Langevin runs (the generation of initial conditions) and Hamilton runs (integration of the equations of motion). Spatial correlation functions used for the study of screening properties were averaged over the Langevin runs. The Langevin runs lasted typically 120 (in lattice units), which we found sufficient to decorrelate observables such as the ‘link’ $\text{Tr } \phi^\dagger U \phi$, while the Hamilton runs lasted in most cases several thousand. Details on the statistics will be given below where we summarize the parameter values in Table 2.

The spatial correlation in the 3-direction at distance d , of a local observable $O_{\mathbf{x}}$ at zero transverse momentum, was estimated as follows,

$$G_O(d) = \frac{1}{N} \sum_{x_3} \left[\overline{\tilde{O}_{x_3+d} \tilde{O}_{x_3}} - \overline{\tilde{O}_{x_3+d}} \overline{\tilde{O}_{x_3}} \right], \quad (13)$$

$$\tilde{O}_{x_3} = \frac{1}{\sqrt{N^2}} \sum_{x_1, x_2} O_{x_1, x_2, x_3}, \quad (14)$$

where the bar denotes the average over the Langevin bins (we used periodic spatial boundary conditions). In the limit of an infinite number of bins $\overline{O_{\mathbf{x}}} \rightarrow \langle O_{\mathbf{x}} \rangle$ which is independent of \mathbf{x} . For the Higgs mode we used $O_{\mathbf{x}} = H_{\mathbf{x}}$ (cf. (12) and we averaged the correlators over the three different directions (3, 1, and 2). For the W -mode we used the transverse components $O_{\mathbf{x}} = \sum_{\alpha=1}^3 W_{k\mathbf{x}}^\alpha$, $k = 1, 2$, which leads to a $G_{W_k}(d)$ independent of k , and we averaged over k , $G_W(d) = [G_{W_1}(d) + G_{W_2}(d)]/2$, and over the three different directions. (The summation over $\alpha = 1, 2, 3$ picks out a particular direction in isospin space; we could have improved statistics a little by correlating and averaging the α ’s as well).

For the time dependent correlators we used microcanonical averaging over the Hamilton parts of the simulation in addition to canonical averaging over initial conditions at the end of the Langevin parts. The autocorrelation functions were constructed analogously to (13),

$$C_O(t) = \frac{1}{t_b} \int_0^{t_b} dt_0 \left[\overline{O(t_0+t)O(t_0)} - \overline{O(t_0+t)} \overline{O(t_0)} \right], \quad (15)$$

$\bar{\beta}$	N	\bar{v}^2	T/m_H	T/T_c	t_{run}	nc(sc)	nc(pl)
6	24	0.263	-	-	640	35	22
8	24	0.263	-	-	320	41	51
10	24	0.263	3.46	1.61	1280	24	48
11	24	0.263	2.64	1.23	400	89	86
12	24	0.263	2.15	1	1500	30	29
12.5	24	0.263	1.98	0.92	6400	35	30
13	24	0.263	1.82	0.85	5000	42	42
14	24	0.263	1.59	0.74	6400	15	18
20	24	0.263	0.88	0.41	1000	15	15
13'	20	0.263	1.81	0.85	5000	40	11
21.7	32	0.156	1.67	0.78	7000	31	12
11'	20	0.263	2.63	1.23	2500	57	56
11*	20	0.246	3.26	1.52	3000	61	61
18.3	32	0.156	3.26	1.52	2500	37	21

Table 2: Summary of parameter values and statistics. The prime or * on $\bar{\beta}$ distinguishes different N and \bar{v}^2 .

where $0 < t < t_{\text{run}} - t_b$. Here the bar denotes the canonical average and t_{run} is the maximum time in the Hamilton run. When the number of initial conditions goes to infinity this expression approaches the exact $\langle O(t)O(0) \rangle - \langle O \rangle^2$. For the determination of the plasmon properties we used for O the zero momentum projections

$$W_k^\alpha = \frac{1}{\sqrt{N^3}} \sum_{\mathbf{x}} W_{k\mathbf{x}}^\alpha, \quad H = \frac{1}{\sqrt{N^3}} \sum_{\mathbf{x}} H_{\mathbf{x}}, \quad (16)$$

and for W we averaged over k and α .

4 Results for the screening correlators

Table 2 gives a summary of the parameter values used in our simulations. The values of T/m_H correspond to eq. (7). (For $\bar{\beta} = 4, 8$ the lattice spacing is so large that eq. (7) breaks down; note that $O(a)$ terms are neglected in $[\dots]$.) The ratios T/T_c have been added for convenience and follow simply by division by $T_c/M_H(\mu_{T_c})$ in Table 1, i.e. without taking into account the running of $m_H(\mu_T)$ with T . The time t_{run} is the length of the Hamilton runs used in the computation of the autocorrelation functions, in lattice units; nc(sc) and nc(pl) are the number configurations (number of Langevin runs) used in the calculation of the screening and plasmon properties, respectively.

$\bar{\beta}$	am_H	am_W	m_H/g^2T	m_W/g^2T
6	1.2(6)	1.5(18)	1.8(9)	2.3(27)
8	1.12(20)	1.04(58)	2.24(40)	2.1(12)
10	0.68(4)	1.34(28)	1.7(1)	3.4(7)
11	0.46(3)	0.88(14)	1.27(8)	2.4(4)
12	0.146(29)	0.37(2)	0.44(9)	1.11(6)
12.5	0.22(3)	0.38(1)	0.69(9)	1.19(3)
13	0.28(3)	0.35(2)	0.91(9)	1.14(7)
14	0.34(1)	0.41(2)	1.19(4)	1.44(7)
20	0.59(5)	0.50(2)	2.95(25)	2.5(1)
13'	0.26(2)	0.39(3)	0.85(7)	1.27(10)
21.7	0.22(2)	0.25(2)	1.19(11)	1.36(11)
11'	0.44(3)	0.96(11)	1.21(8)	2.64(30)
11*	0.59(5)	1.06(20)	1.62(14)	2.92(55)
18.3	0.31(3)	0.65(10)	1.42(14)	2.97(46)

Table 3: Results for the screening masses.

We first made a scanning simulation on the $N = 24$ lattice with varying $\bar{\beta}$ and \bar{v}^2 fixed at 0.263, its value for $\bar{\beta}_c = 12$. This means the temperature varied as shown in Table 2. By fitting the correlation functions $G_{H,W}(d)$ to $A \cosh[am(d - N/2)]$ we obtained the screening masses m shown in Table 3.

We made a least squares fit to the data at $d = 3 - 5$, which led to reasonable looking fits, and the errors were obtained with the jackknife method. This procedure is of course not state of the art as in [20], but we only wanted to get an overall impression of the data at the chosen parameters using a moderate amount of computational effort.

After this scan we decided to concentrate on two values of $\bar{\beta}$ corresponding to two values of the lattice spacing, in the Higgs phase as well as in the confinement phase. The parameters \bar{v}^2 and N were changed accordingly such that the two $\bar{\beta}$ values tentatively describe the same physical situation. The guiding parameter values were those of the transition obtained nonperturbatively in [25], which are shown in Table 1: $(\bar{\beta}, N, \bar{v}^2) = (12, 20, 0.263)$ and $(20, 32, 0.156)$. Modulo scaling violations this corresponds to a ratio of lattice spacings $12/20 = 0.6$ at approximately the same physical volume ($20/32 = 0.625$). The new parameters in the Higgs phase were obtained by changing $\bar{\beta} = 12 \rightarrow 13$ and $\bar{\beta} = 20 \rightarrow 21.7 \approx 13/0.6$, keeping fixed the corresponding N and \bar{v}^2 . These pairs of $(\bar{\beta}, N, \bar{v}^2)$ values correspond roughly to the same T/M_H (using the matching formula (7), as shown in Table 2 (cf. $\bar{\beta} = 13$ and 21.7)). The same parameter combinations were used in [10] for the computation of the Chern-Simons diffusion rate. Similarly the

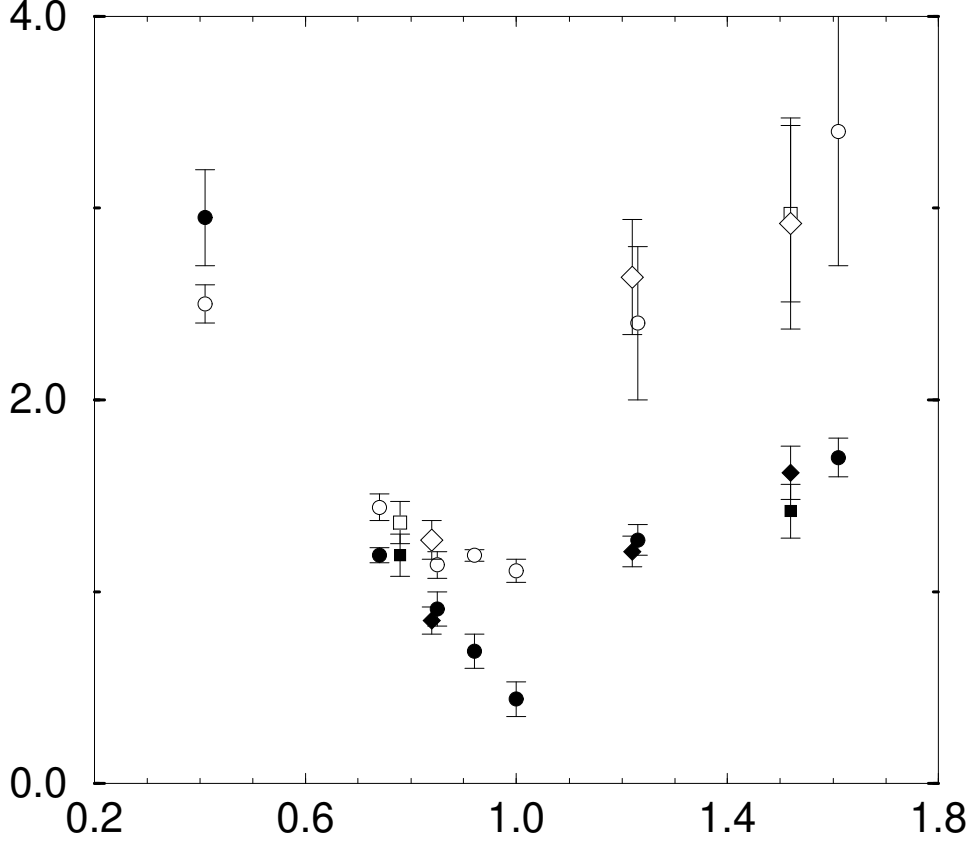


Figure 1: Screening masses $m_{H,W}/g^2T$ versus T/T_c . Solid symbols correspond to H , open symbols to W ; circle: 24^3 data; diamond: 20^3 data; square: 32^3 data.

confinement phase parameters were obtained by changing $\bar{\beta} = 12 \rightarrow 11$ and $\bar{\nu}^2 = 20 \rightarrow 18.3 \approx 11/0.6$, again without changing the corresponding N and $\bar{\nu}^2$. However, here the matching formula (7) gives a larger mismatch in T/m_H (cf. $\bar{\beta} = 11'$, 18.3 in Table 2). To keep T/m_H fixed more precisely we have to adjust $\bar{\nu}^2$. Therefore we also did measurements in the confinement phase at $(\bar{\beta}, N, \bar{\nu}^2) = (11, 20, 0.246)$, for which $\bar{\nu}^2$ was chosen such that T/m_H equals its value at $(\bar{\beta}, N, \bar{\nu}^2) = (18.3, 32, 0.156)$.

Table 3 also shows the results for the screening masses of these additional simulations. We fitted the data at $d = 3 - 5$ for $N = 20$ and at $d = 4 - 7$ for $N = 32$. Fig. 1 shows the screening masses in physical units, m/g^2T , versus T/T_c . The transition at $T = T_c$ is clearly visible and we also see the ratio m_H/m_W approaching 1 at low temperatures, as expected from the choice $\bar{\lambda} = 1/2$. (The

dimensional reduction approximation is of course questionable at the most left points where T/M_H is only 0.88.) We observe no significant volume dependence away from the phase transition in the data at $T/T_c = 0.85$ and 1.23. The data at $T/T_c = 1.52$ ($\bar{\beta} = 11^*$ and 18.3) show reasonable lattice spacing independence (recall that the ratio of lattice spacings is 0.6). The difference in m/g^2T between $\bar{\beta} = 13$ and 21.7 is evidently due to the difference in physical temperatures, $T/T_c = 0.84$ and 0.78, and not a signal of lattice spacing dependence.

$\bar{\beta}$	$am_{\text{eff } H}$	$am_{\text{eff } W}$	$m_{\text{eff } H}/g^2T$	$m_{\text{eff } W}/g^2T$
13'	0.24(2)	0.43(4)	0.78(7)	1.40(13)
21.7	0.18(3)	0.27(3)	0.98(16)	1.46(16)
11'	0.64(5)	1.65(14)	1.76(14)	4.5(4)
11*	0.64(4)	1.84(13)	1.76(11)	5.1(4)
18.3	0.32(5)	1.26(11)	1.46(23)	5.8(5)

Table 4: Effective screening masses from eq. (18).

We also like to mention our experience with a momentum space analysis of the correlation functions, which has been popular in numerical studies of the Higgs-Yukawa sector of the Standard Model. This analysis is based on the Fourier transform of $G_{H,W}(d)$,

$$G_{H,W}(p) = \sum_d e^{-ipd} G_{H,W}(d). \quad (17)$$

Here p is one of the lattice momenta, $ap = 2\pi n/N$, $n = 0, 1, \dots, N-1$. Within statistical errors these are real functions of p . We deduced effective screening masses m_{eff} from the expansion

$$G(p)^{-1} = Z^{-1}[a^2 m_{\text{eff}}^2 + p^2 + O(p^4)], \quad (18)$$

by fitting G^{-1} as a function of $\hat{p}^2 \equiv 2 - 2\cos ap$ to a straight line, using two of the lower p values ($n = ap/(2\pi/N) = 0, 1$ and 1,2). The resulting effective screening masses (cf. Table 4) tend to be significantly larger than the true screening masses above, especially for W in the confinement phase, for which $G^{-1}(p)$ shows strong curvature. (Fitting more data points to a quadratic function had no significant effect on the results.) The effective masses are expected to be a good approximation to the screening masses only in case of pole dominance of $G(p)$, which evidently is not the case for W in the confinement phase.

It is known that in the Higgs phase the simple fields (11, 12) which we use perform reasonably well in creating dominantly the H and W out of the vacuum, but in the confinement phase they easily create also excited states with the same quantum numbers as H and W (for a recent study see [20]). The excited state

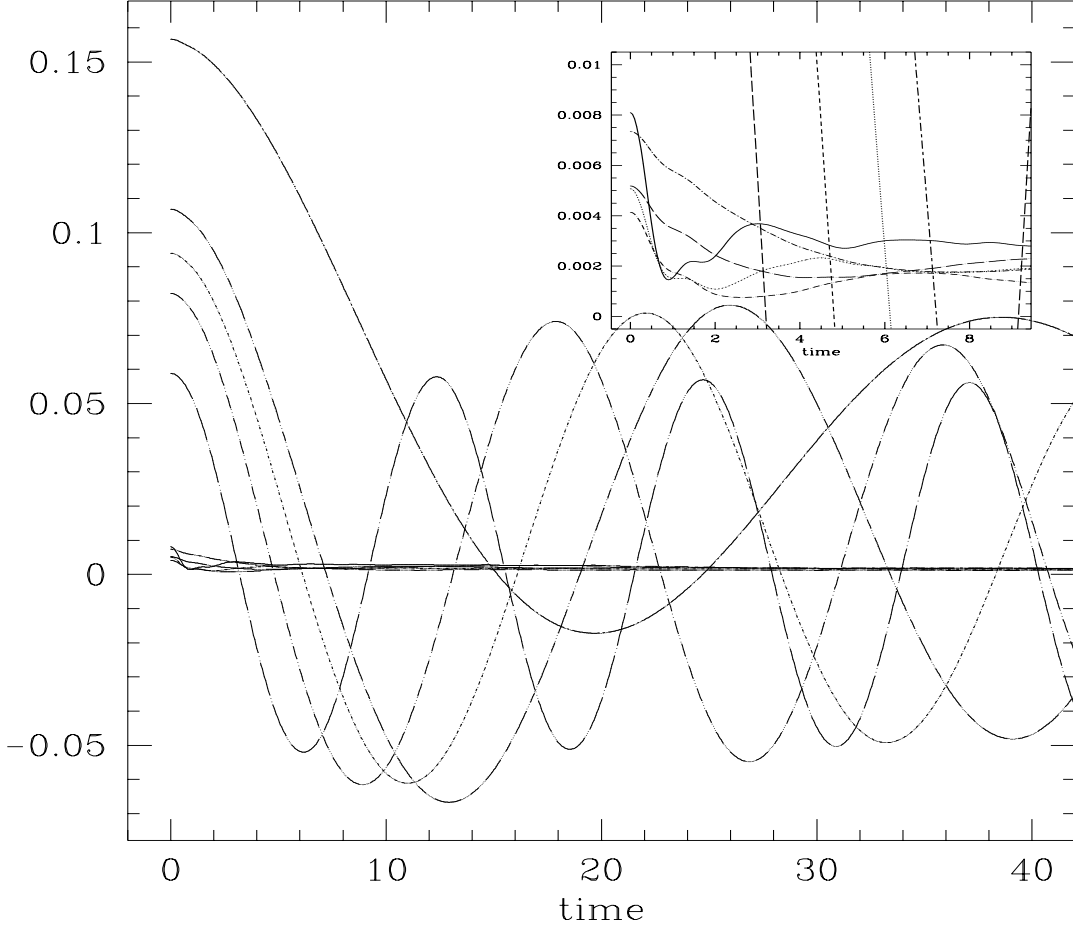


Figure 2: Scan of $C_H(t)$ from the 24^3 data. The first minima in $t > 5$ are in order of decreasing $\bar{\beta} = 20, 14, 13, 12.5, 12$. The lines in the middle of the C_H plot are for $\bar{\beta} < 12$, shown enlarged in the insert.

contribution weakens of course pole dominance. To do better one has to use more sophisticated observables instead of the simple $H_{\mathbf{x}}$ and $W_{k\mathbf{x}}^\alpha$, e.g. the smeared fields used in [20].

5 Results for the plasmon correlators

The results in the previous section for the screening properties of H and W give us a feeling how well we are doing in a familiar situation, in the theoretical framework of dimensional reduction. We now turn to the time dependent correlation functions, for which we are on less established ground. Figs. 2 and 3 show an initial scan of the autocorrelation functions $C_H(t)$ and $C_W(t)$ for various $\bar{\beta}$ at

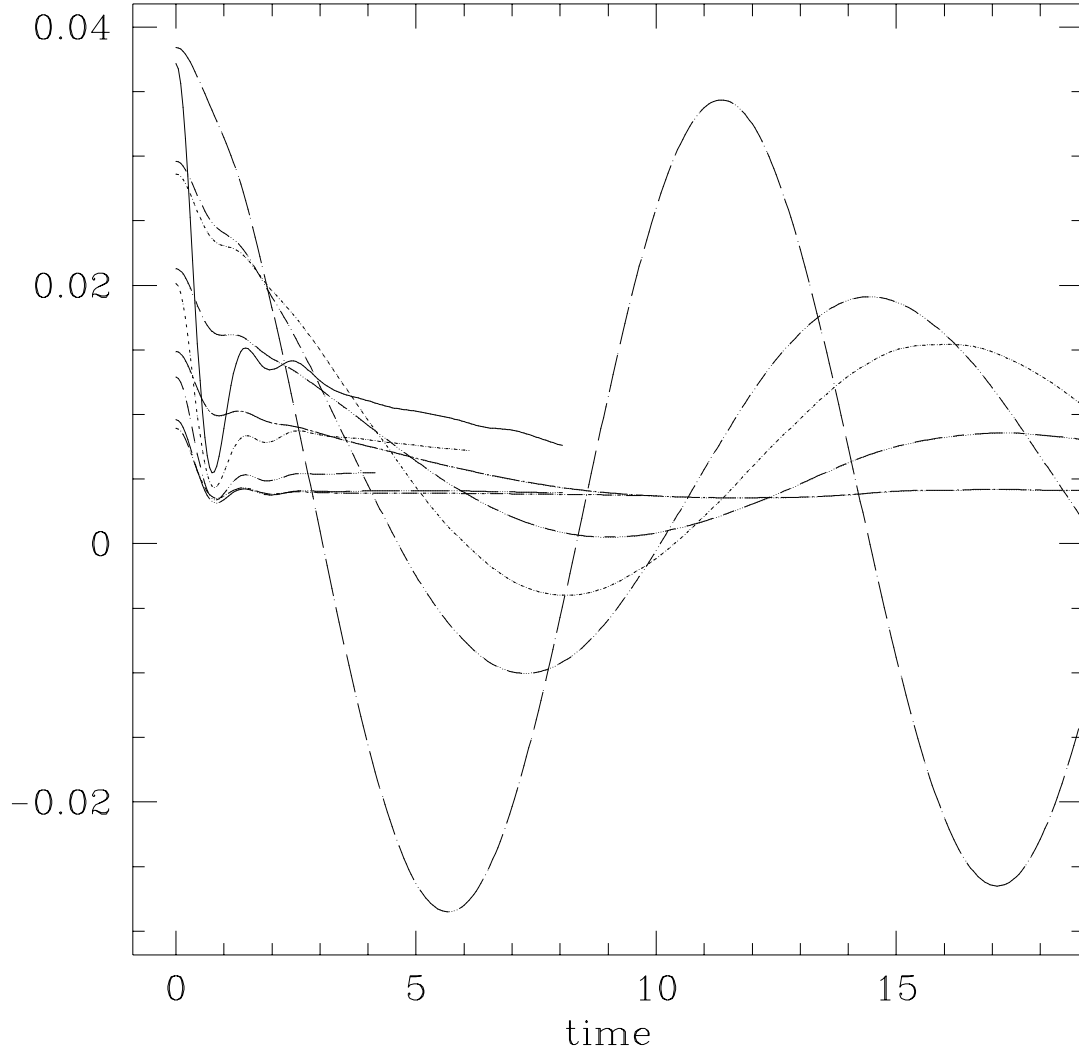


Figure 3: Scan of $C_W(t)$ from the 24^3 data. The first minima in $t > 5$ are in order of decreasing $\bar{\beta} = 20, 14, 13, 12.5, 12$. The lines ending before $t = 10$ are for $\bar{\beta} < 12$; bottom to top ($t = 4$): $\bar{\beta} = 11$ (touching the minimum of $\bar{\beta} = 12$), 10 (nearly coinciding with 11), 8, 6 and 4.

fixed $\bar{v}^2 = \bar{v}_c^2(\bar{\beta} = 12)$ on the 24^3 lattice. The horizontal time scale is in lattice units (i.e. (number of time integration steps) \times (step size) as it appears in the computer code). The time in lattice units can be converted to physical units by multiplication with e.g. the temperature in lattice units. We see the period of the oscillations increasing as we approach the transition at $\bar{\beta} = 12$ from above (from the Higgs side)².

In the H case (Fig. 2) there is a drastic change of behavior below $\bar{\beta} = 12$ (the confinement side), where the signal is much smaller. As the insert shows the data here is very noisy, although we think the very short time ($t < 2$) data is still relevant, because short times allow for more microcanonical averaging. Notice the oscillations in this very short time region.

For W (Fig. 3) the transition appears more gradual. As $\bar{\beta}$ is lowered down from 20, small oscillations in the small time region ($t < 2$) appear already in the Higgs phase. When $\bar{\beta}$ is decreased further below 12 the initial oscillations increase somewhat and so does the slope afterwards, which is nearly zero for $\bar{\beta} = 11, 10, 8$. In this case we have stopped the drawing of the curves at early times because the statistical noise would be overwhelming.

To extract a plasmon frequency and damping rate we fit the data in the Higgs phase to the simple asymptotic form

$$Re^{-\gamma} \cos(\omega t + \alpha) + C. \quad (19)$$

For a free scalar field we would have $R = T/m^2$, $\gamma = C = 0$. With interactions the form (19) is expected to be a good approximation in case of small damping [30]. It turns out that the phase α is not really needed and may be set equal to zero. In the confinement phase the signal of our 24^3 data is too noisy for a quantitative analysis. For the Higgs phase the 24^3 data led to the plasmon parameters shown in Tables 5 and 6. The errors are based on jackknifing with respect to the initial conditions. The damping rate γ is sensitive to the beginning of the fitting range, the fits above started roughly from the third maximum of $C_H(t)$ (the first maximum is at $t = 0$).

We increased the numerical effort on the confinement phase parameters values $\bar{\beta} = 11', 11^*$ and 18.3 and did similar runs for $13'$ and 21.7. Fig. 4 shows the autocorrelation function $C_H(t)$ in the Higgs phase for $\bar{\beta} = 13'$ and 21.7. A fit to (19) starting roughly at the third maximum led to the plasmon parameters shown in Tables 5 and 6. Figure 5 shows the W -autocorrelation functions in the Higgs phase. It is clear that the W damping rate is considerably larger than for H and to avoid running into noise we had to lower the starting time of the fit to (19) down to roughly the second maximum. The results in physical units are shown in Figs. 6 and 7. From the smooth adjustment of the $\bar{\beta} = 21.7$ (32^3) data with the $\bar{\beta} = 13'$ and 13 (20^3 and 24^3) data it follows that the plasmon frequencies and

²The curves at $\bar{\beta} = 12$ belong clearly to the Higgs phase sequence, which suggests that $\bar{\beta}_c$ is actually slightly smaller than 12.

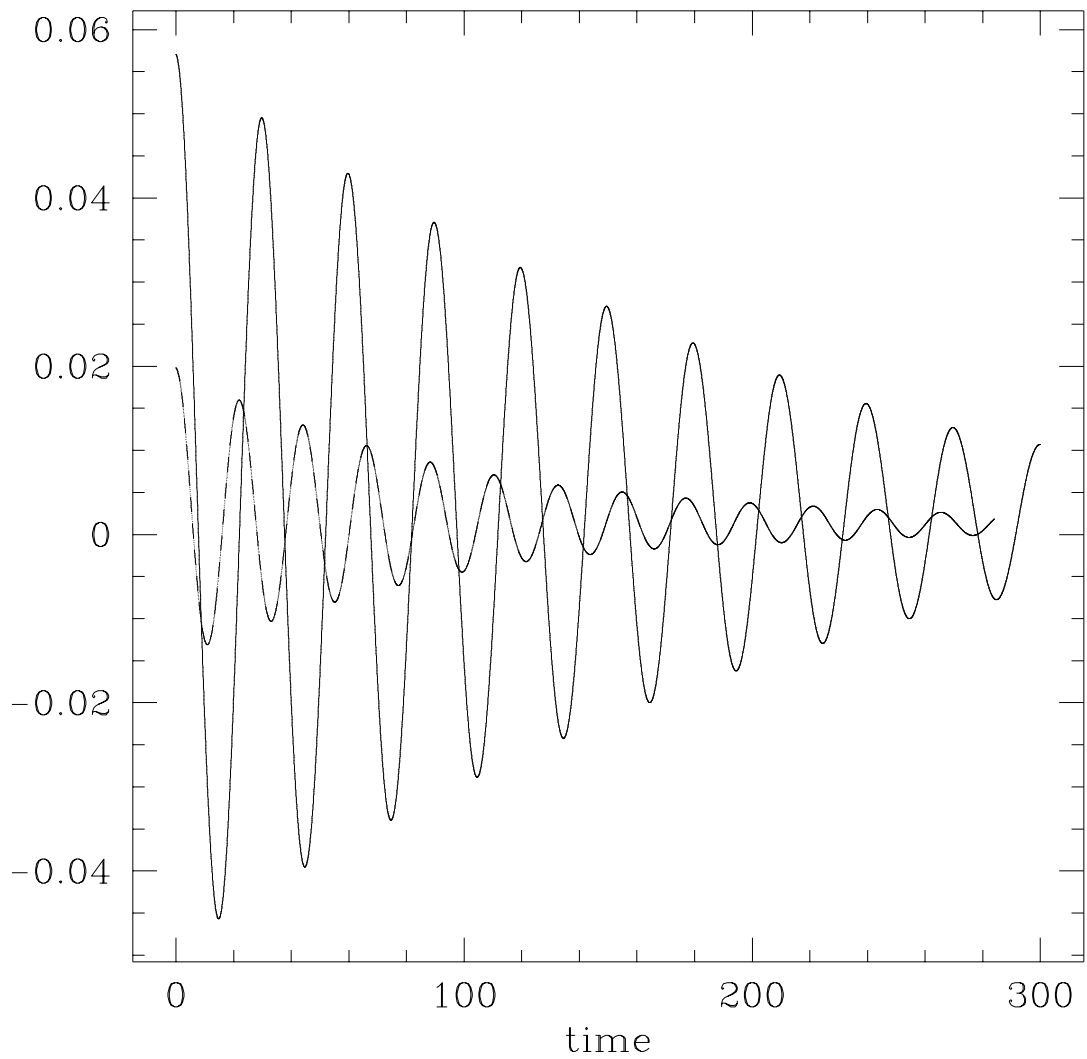


Figure 4: The autocorrelator $C_H(t)$ in the Higgs phase for $\bar{\beta} = 13'$ and 21.7.

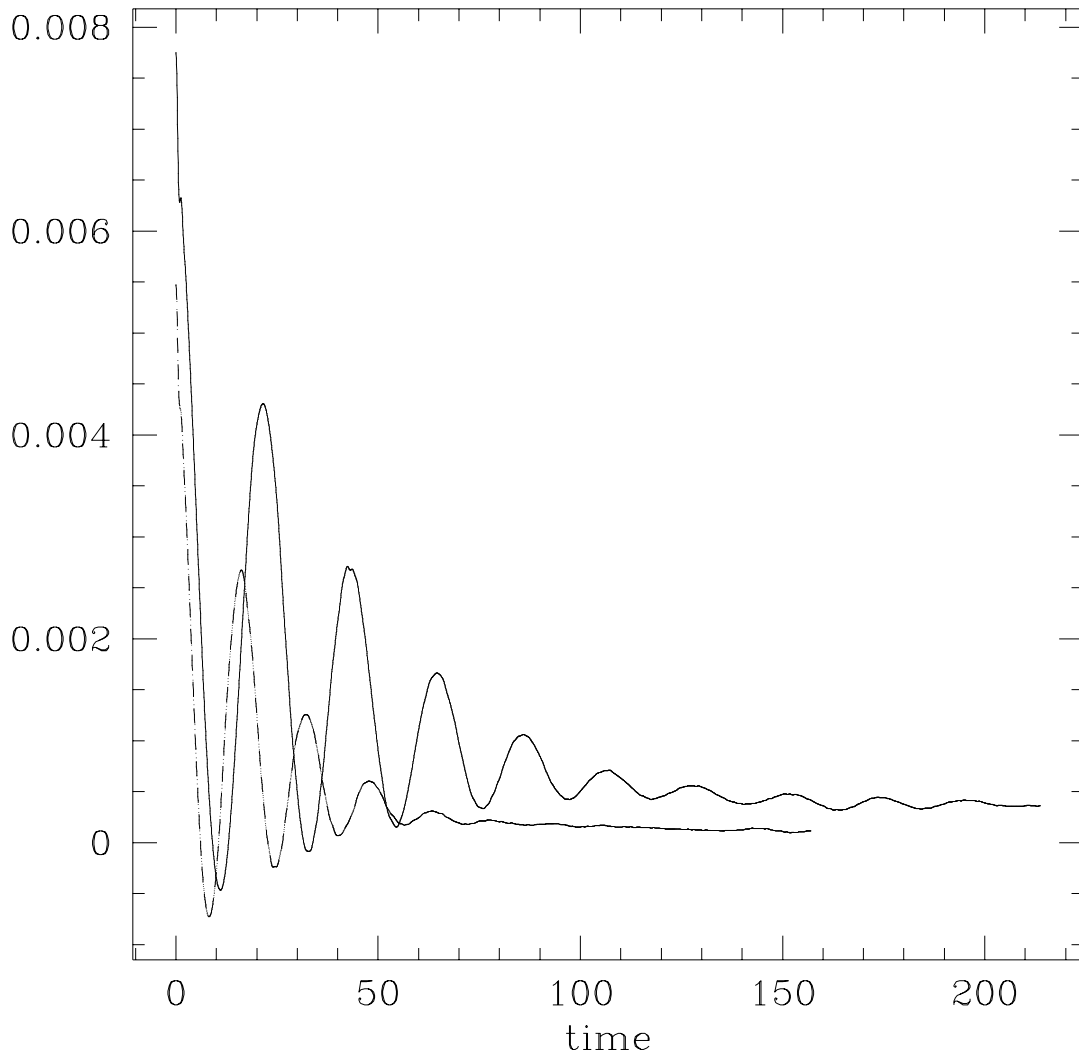


Figure 5: The autocorrelator $C_W(t)$ in the Higgs phase for $\bar{\beta} = 13'$ and 21.7.

$\bar{\beta}$	$a\omega_H$	$a\omega_W$	ω_H/g^2T	ω_W/g^2T
12	0.16(1)	—	0.48(3)	—
12.5	0.24(1)	0.35(2)	0.75(3)	1.09(6)
13	0.28(2)	0.38(2)	0.91(7)	1.24(7)
14	0.350(4)	0.430(6)	1.23(2)	1.51(2)
20	0.508(2)	0.551(2)	2.54(1)	2.76(1)
13'	0.284(5)	0.382(5)	0.92(2)	1.24(2)
21.7	0.210(2)	0.296(2)	1.14(1)	1.61(1)
11'	0.33(3)	—	0.91(8)	—
11*	0.44(3)	—	1.21(8)	—
18.3	0.23(2)	—	1.05(9)	—

Table 5: Results for the plasmon frequencies.

damping rates are nearly lattice spacing independent. The constant C of the fits is non-zero. However, we have seen the autocorrelators to tend to zero at very large times.

In the confinement phase the behavior is qualitatively different. Fig. 8 shows that $C_H(t)$ still has roughly the form (19), but with an average C that gets significantly smaller in a period of oscillation. A reasonable fit to the data could be obtained by letting $C \rightarrow Ct^{-\delta}$ in a region starting a little before the second maximum to times where the oscillations appear to have died out, judging by eye. An example of such a fit is shown in figure 8. The large statistical errors for C_H in the Higgs phase show up in the lack of smoothness in the data and the resulting jackknife error on γ_H is very large. The results are in Tables 5, 6 and Figs. 6 and 7. The fitted power δ is about 0.2 – 0.4. For larger times ($t > 100$ for 11*) the power δ appears to increase, as shown in the double logarithmic plot Fig. 9, which also shows that there is no good evidence for exponential behavior. Asymptotically one would expect the $t^{-3/2}$ behavior familiar from zero temperature [30].

The W autocorrelator behaves very differently. Fig. 10 shows what looks like $C_H(t)$ in Fig. 8, except that the time scale has shrunk by an order of magnitude. The periods of the oscillations are of order 1, which suggests ω 's of order 2π and also the γ 's appear to be very large in lattice units. There is clearly no scaling in this time interval since the period of the oscillation hardly changes as $\bar{\beta}$ increases. We recall that the oscillations start already in the Higgs phase quite far from the phase transition, as mentioned above after introducing Fig. 3. They are not analogous to those of $C_H(t)$ in Fig. 8, but of $C_H(t)$ in the insert in Fig. 2. The small time oscillations correspond to energies of the order of the cutoff and must be considered as lattice artefacts.

Fig. 11 shows the larger time region on a logarithmic scale. We see good evidence for exponential behavior. A power behavior appears to be excluded in

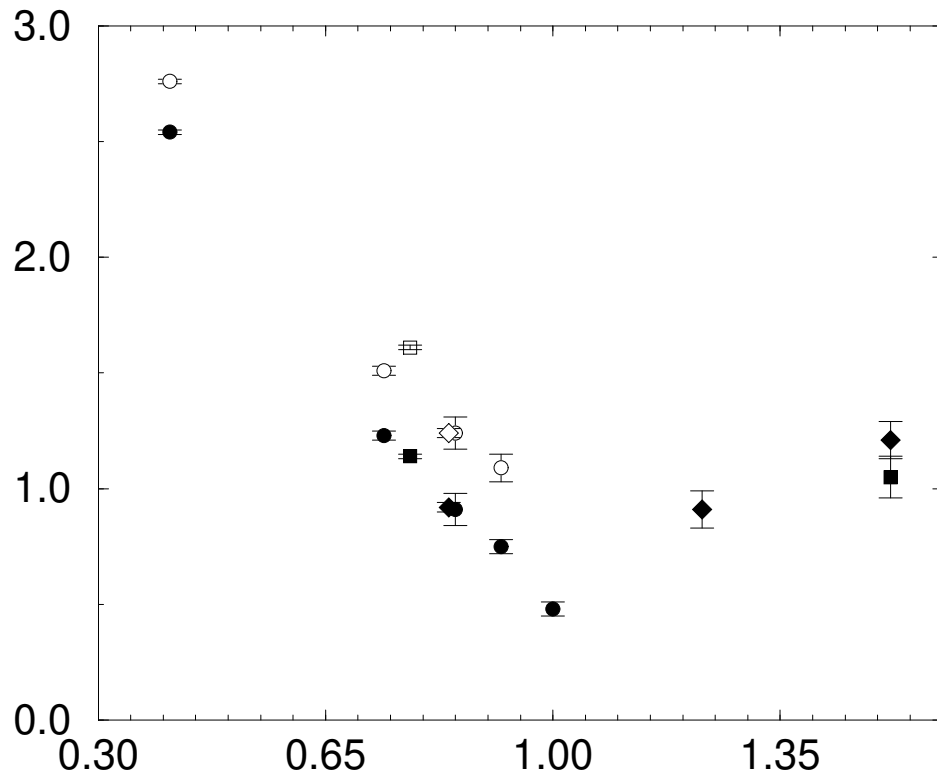


Figure 6: Plasmon frequencies ω/g^2T versus T/T_c . Solid symbols correspond to H , open symbols to W ; circle: 24^3 data; diamond: 20^3 data; square: 32^3 data.

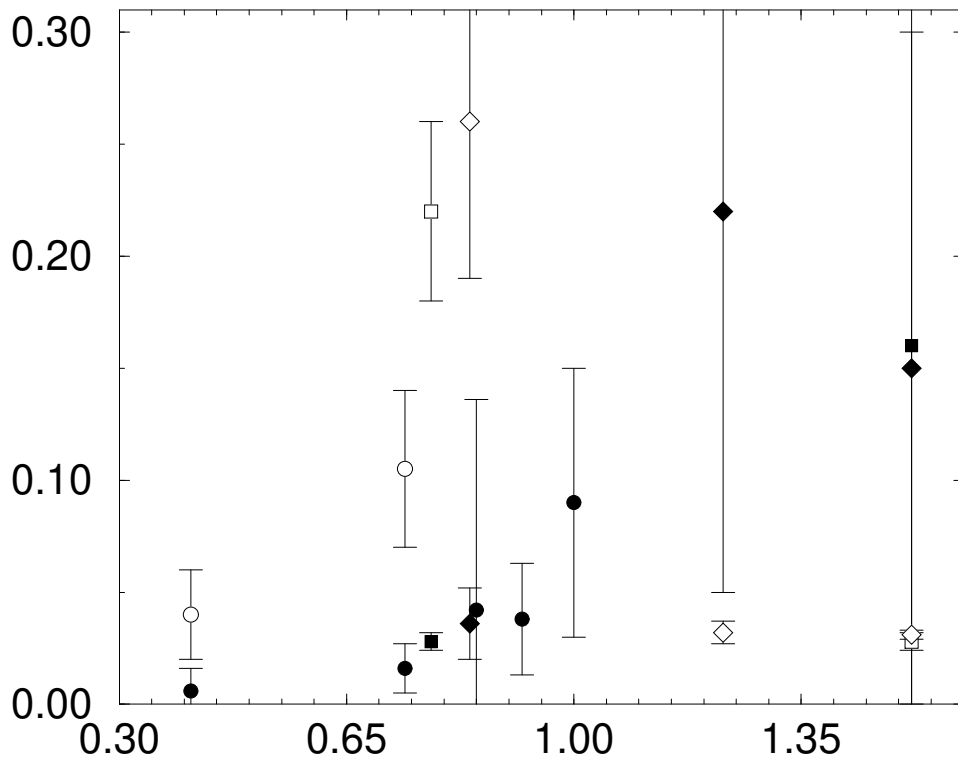


Figure 7: Damping rates γ/g^2T versus T/T_c . Solid symbols correspond to H , open symbols to W ; circle: 24^3 data; diamond: 20^3 data; square: 32^3 data.

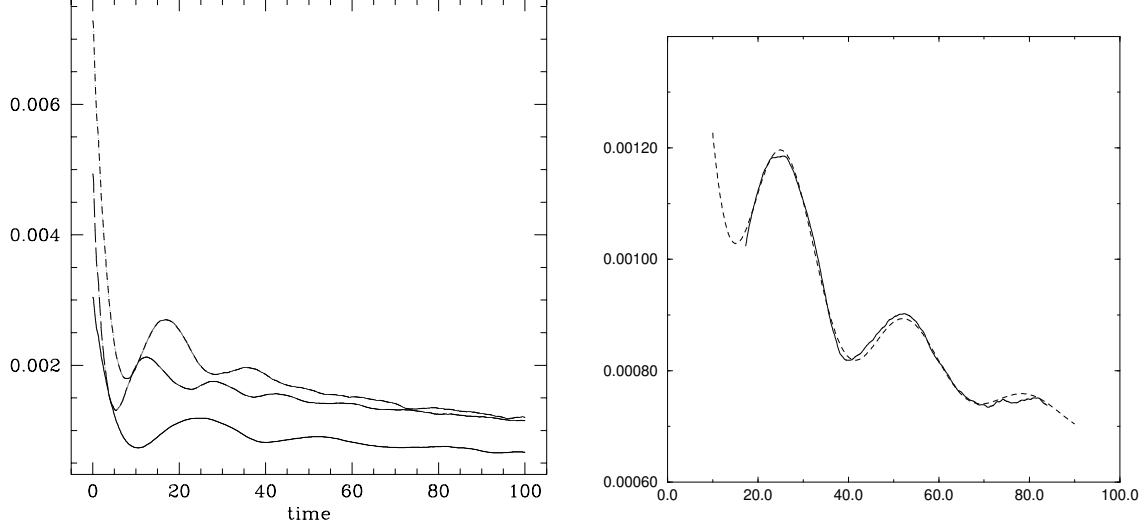


Figure 8: Left: $C_H(t)$ in the confinement phase; $\bar{\beta} = 18.3, 11^*$ and $11'$ in ascending order. Right: fit (dashed curve) to the data at $\bar{\beta} = 18.3$; the fitting region corresponds to the data shown.

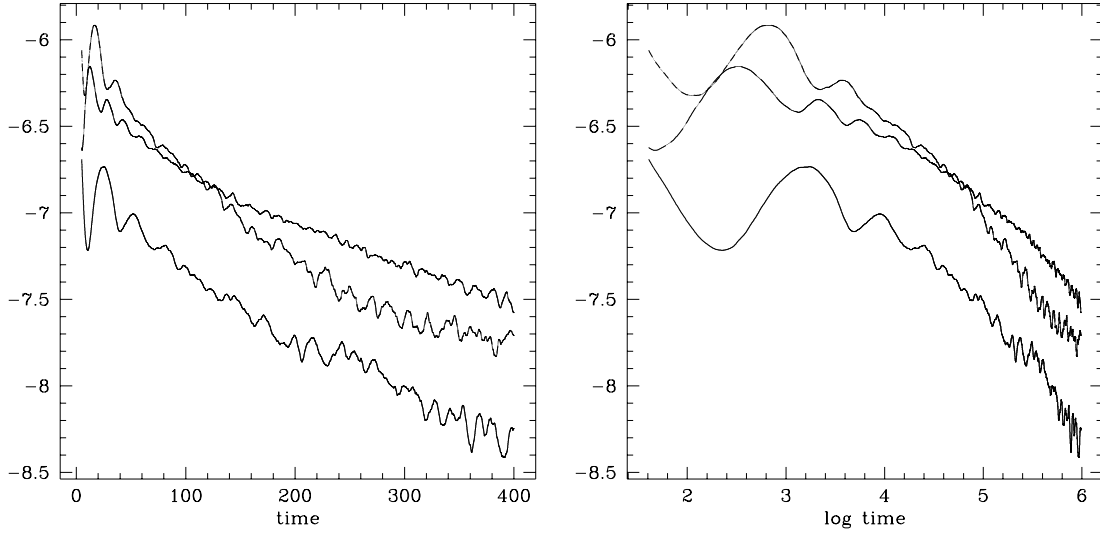


Figure 9: $\ln C_H(t)$ versus t (left) and $\ln C_H(t)$ versus $\ln t$ (right) in the confinement phase.

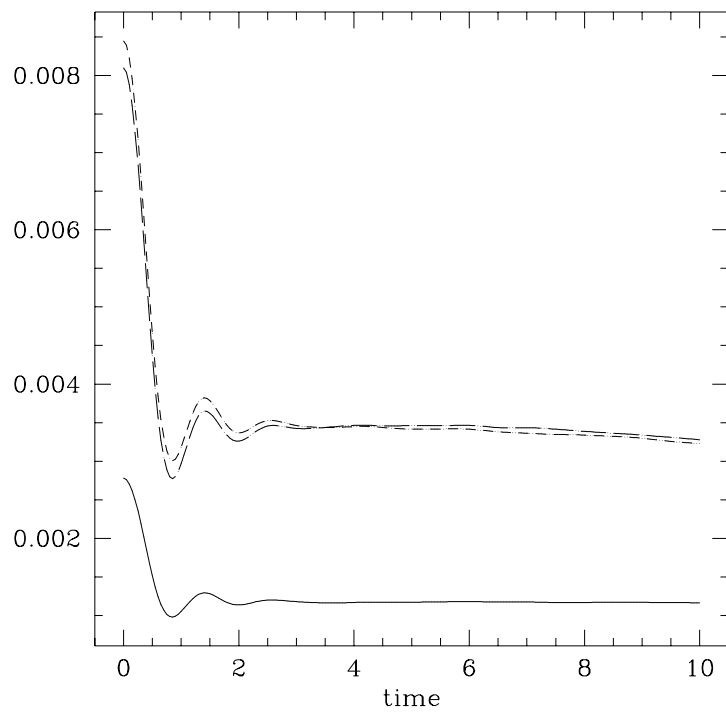


Figure 10: Short time behavior of $C_W(t)$ in the confinement phase. Top to bottom ($t \approx 1$): $\bar{\beta} = 11'$, 11^* and 18.3 .

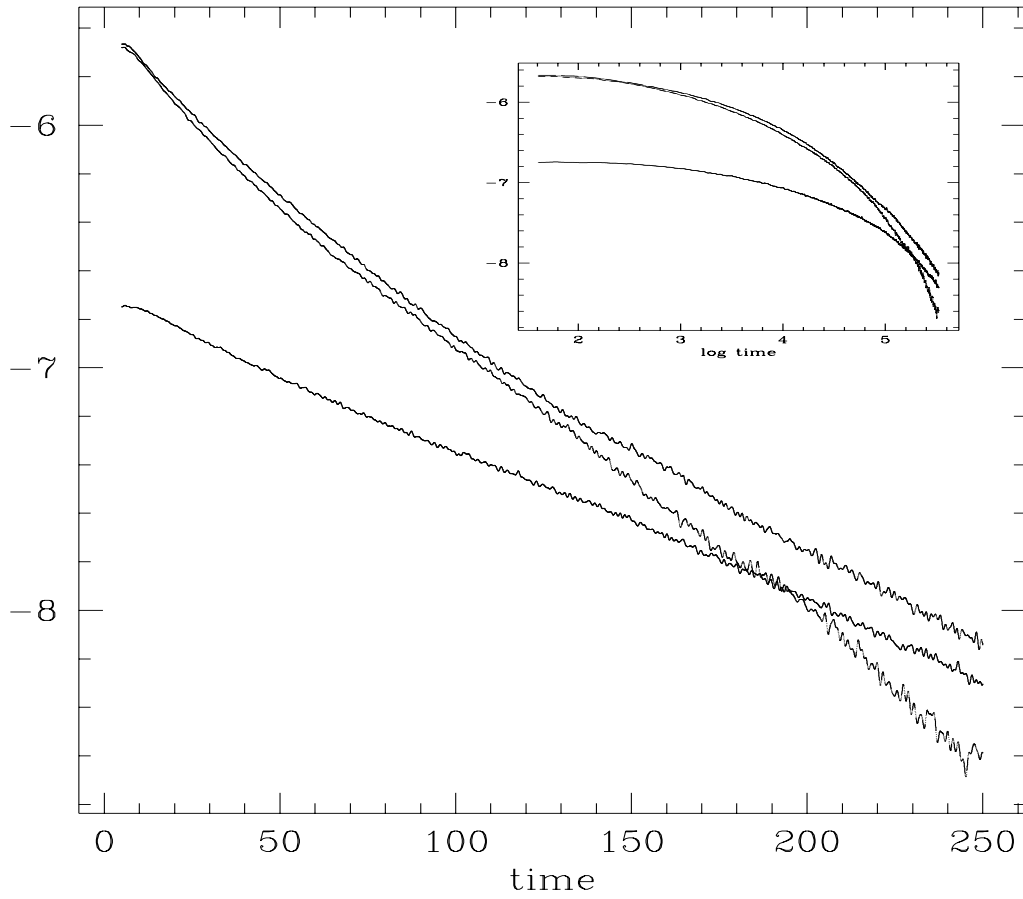


Figure 11: Plot of $\ln C_W(t)$ in the confinement phase for larger times; $\bar{\beta} = 11'$ (top), 11^* (middle) and 18.3 (bottom). The insert shows the same time interval on a double logarithmic plot.

$\bar{\beta}$	$a\gamma_H$	$a\gamma_W$	γ_H/g^2T	γ_W/g^2T
12	0.03(2)	—	0.09(6)	—
12.5	0.012(8)	0.09(9)	0.038(25)	0.28(28)
13	0.013(29)	0.04(5)	0.042(94)	0.13(16)
14	0.0045(31)	0.03(1)	0.016(11)	0.105(35)
20	0.0012(19)	0.008(4)	0.006(10)	0.04(2)
13'	0.011(5)	0.08(2)	0.036(16)	0.26(7)
21.7	0.0052(8)	0.041(8)	0.028(4)	0.22(4)
11'	0.079(61)	0.0116(17)	0.22(17)	0.032(5)
11*	0.053(55)	0.0111(6)	0.15(15)	0.031(2)
18.3	0.036(40)	0.0062(8)	0.16(18)	0.028(4)

Table 6: Results for the damping rates.

the time range shown (cf. insert). The drop of $C_W(t)$ can be fitted to an exponential with a damping rate in physical units that is lattice spacing independent, within errors, as shown in Table 6 and Fig. 6. On the other hand, the slopes of $\bar{\beta} = 11'$ and 11^* are equal within errors which suggests that the W dynamics is practically independent of the scalar field dynamics in the confinement phase. A similar effect has been noticed for the screening lengths, see e.g. [20]. There appear to be no oscillations in the exponential regime. At very large times we found irregular oscillations with a period of order 600 (18.3 data), indicating a plasmon frequency of order 0.01, but the statistics is insufficient to be able to say anything more definite. We tentatively conclude that the W plasmon frequency is very small, possibly zero.

6 Discussion

We have learned that numerical computations of real time correlation functions in hot SU(2)-Higgs theory are feasible in the classical approximation. In this exploratory study we have not indicated statistical errors in our plots of the correlation functions. In most cases these are quite reasonable, but in some they would swamp the data lines, e.g. for H in the confinement phase. However, we believe the jackknife errors given in Tables 5, 6 and Figs. 6, 7 are mostly realistic and they can be improved with a reasonable increase of computational effort. The errors on γ_H appear to be overestimated, but this can only be clarified by increasing statistics. Systematic errors are harder to assess. It is one thing to compute an autocorrelation function, and quite another to extract plasmon parameters from these when the damping rate is relatively large. But then the very relevance of such concepts is questionable in case of strong damping.

We are encouraged by the fact that the results are compatible with lattice spacing independence, within errors. It suggests that the time dependent theory is indeed renormalizable and that order a effects are small. The situation here is different from that of Chern-Simons diffusion, because the observables are different. There is no reason to suspect that the large (in lattice units) time behavior of correlation functions can suffer from lattice artefacts in a renormalizable theory when the lattice spacing goes to zero.

As argued in the Introduction, comparison with analytical results is to be done in the Higgs phase. The numerical damping rates in the Higgs phase compare reasonably well: the $\bar{\beta} = 21.7$ ($T/T_c = 0.78$) data give $\gamma_W/g^2T = 0.22(4)$ and $\gamma_H/g^2T = 0.028(4)$, to be compared with 0.176 and ≈ 0.02 , respectively [31, 32]. Of course, these values will depend on the distance from the transition at T_c , even more so for the plasmon frequencies (cf. Figs. 6, 7).

The damping γ_H increases substantially when the temperature is raised above T_c , while γ_W drops dramatically. Both damping rates appear to be roughly temperature independent in the confinement phase, although the errors on γ_H are much too large for a definite conclusion.

One of the assets of the numerical method is its ability for dealing with dynamical mass generation. Starting from a classically ‘massless’ theory in the confinement phase one expects to find clearly nonzero values for all the plasmon frequencies, as is the case with the screening masses. We were surprised therefore to find indications in our data for an ω_W in the confinement phase, which is so small that we could not reliably measure it. The ω_H on the other hand show a dip at T_c similar to the screening masses.

Acknowledgement

The numerical simulations made use of the code [24] kindly provided to us by Alex Krasnitz. This work is supported by FOM and NCF, with financial support from NWO.

References

- [1] D.Yu. Grigoriev and V.A. Rubakov, Nucl. Phys. B299 (1988) 67.
- [2] D.Yu. Grigoriev and V.A. Rubakov and M.E. Shaposhnikov, Nucl. Phys. B326 (1989) 737.
- [3] A. Bochkarev and P. de Forcrand, Phys. Rev. D47 (1993) 3476.
- [4] A. Krasnitz and R. Potting, Nucl. Phys. B (Proc. Suppl.) 34 (1994) 613.
- [5] J. Smit and W.H. Tang, Nucl. Phys. B (Proc. Suppl.) 34 (1994) 616.
- [6] P. de Forcrand, A. Krasnitz and R. Potting, Phys. Rev. D50 (1994) 6054.

- [7] J. Smit and W.H. Tang, Nucl. Phys. B (Proc. Suppl.) 42 (1995) 590.
- [8] J. Ambjørn, T. Askgaard, H. Porter and M.E. Shaposhnikov, Phys. Lett. B244 (1990) 479; Nucl. Phys. B353 (1991) 346.
- [9] A. Krasnitz, private communication.
- [10] J. Smit and W.H. Tang, Nucl. Phys. B482 (1996) 265.
- [11] J. Ambjørn and A. Krasnitz, Phys. Lett. B362 (1995) 97.
- [12] N. Turok and G. D. Moore, hep-ph/9608350.
- [13] M.L. Laursen, J. Smit and J.C. Vink, Nucl. Phys. B343 (1990) 522.
- [14] K. Kajantie, M. Laine, K. Rummukainen and M. Shaposhnikov, Nucl. Phys. B458 (1996) 90.
- [15] G. Aarts and J. Smit, hep-ph/9610415.
- [16] W. Buchmüller and O. Philipsen, Nucl. Phys. B443 (1995) 47.
- [17] Z. Fodor, J. Hein, K. Jansen, A. Jaster and I. Montvay, Nucl. Phys. B439 (1995) 147.
- [18] M. Gürtler, E.-M. Ilgenfritz, J. Kripfganz, H. Perlt and A. Schiller, hep-lat/9605042.
- [19] K. Kajantie, M. Laine, K. Rummukainen and M. Shaposhnikov, Nucl. Phys. B466 (1996) 189.
- [20] O. Philipsen, M. Teper and H. Wittig, Nucl. Phys. B469 (1996) 445.
- [21] F. Karsch, T. Neuhaus, A. Patkós and J. Rank, Nucl. Phys. B474 (1996) 217.
- [22] K. Jansen, Nucl. Phys. B (Proc. Suppl.) 47 (1996) 196.
- [23] K. Rummukainen, hep-lat/9608079.
- [24] A. Krasnitz, Nucl. Phys. B455 (1995) 320.
- [25] K. Farakos, K. Kajantie, K. Rummukainen and M. Shaposhnikov, Phys. Lett. B336 (1994) 494.
- [26] K. Kajantie, M. Laine, K. Rummukainen and M. Shaposhnikov, Nucl. Phys. B466 (1996) 189.
- [27] P. Huet and D. Son, hep-ph/9610259.

- [28] C. Hu and B. Müller, hep-ph/9611292.
- [29] P. Arnold, hep-ph/9701393.
- [30] D. Boyanovsky, M. D'Attanasio, H.J. de Vega, R. Holman and D.-S. Lee, Phys. Rev. D52 (1995) 6805.
- [31] E. Braaten and R.D. Pisarski, Phys. Rev. D42 (1990) 2156.
- [32] T.S. Biró and M.H. Thoma, Phys. Rev. D54 (1996) 3465.